A STUDY ON TITANIUM DIOXIDE NANOPARTICLES SYNTHESIZED FROM TITANIUM ISOPROPOXIDE UNDER SILAR-INDUCED GEL METHOD: TRANSITION FROM ANATASE TO RUTILE STRUCTURE.

Agnes C. Nkele[a], Ugochi K. Chime[a], Leonard Asogwa[a], Assumpta C. Nwanya[a,b,c], Uba Nwankwo[a,d], K. Ukoba[e], T.C. Jen[e], M. Maaza[b,c], Fabian I. Ezema[a,b,c,f*]

[a]Department of Physics and Astronomy, University of Nigeria Nsukka, Nigeria
[b]Nanosciences African Network (NANOAFNET), iThemba LABS-National Research Foundation, 1 Old Faure Road, Somerset West, 7129, P.O. Box 722, Somerset West, Western Cape Province, South Africa
[c]UNESCO-UNISA Africa Chair in Nanosciences/Nanotechnology, College of Graduate Studies, University of South Africa (UNISA), Muckleneuk ridge, P.O. Box 392, Pretoria, South Africa
[d]Department of Physics/Geology/Geophysics, Alex Ekwueme Federal University Ndufu-Alike, Ikwo, Ebonyi State, Nigeria
[e]Department of Mechanical Engineering Science, University of Johannesburg Auckland park Johannesburg.
[f]Department of Physics, Faculty of Natural and Applied Sciences, Coal City University, Enugu, Nigeria

GRAPHICAL ABSTRACT

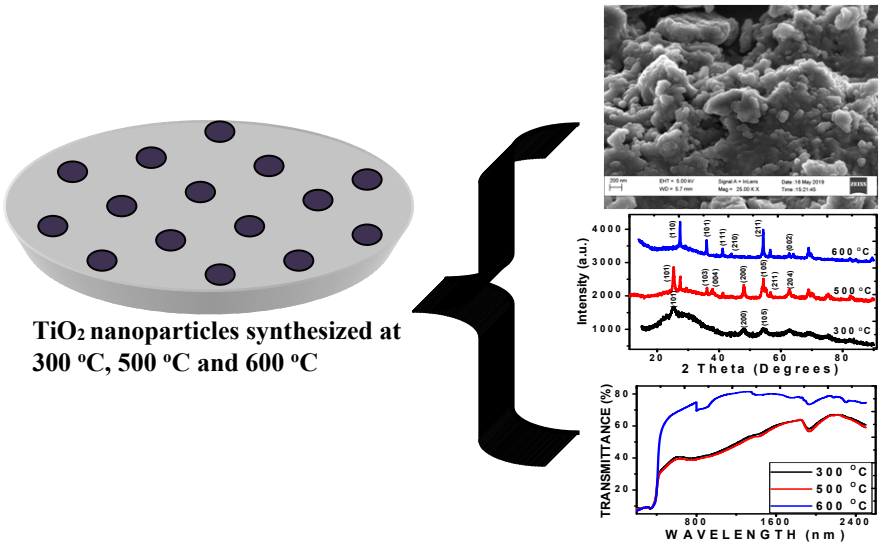

RESEARCH HIGHLIGHTS

- Successful synthesis of TiO_2 nanoparticles at 300 ºC, 500 ºC and 600 ºC by SILAR method.

- Nanospherical balls with an average grain size of about 31 nm were exhibited by the anatase and rutile phases of TiO_2 crystal structure.
- TEM and SAED patterns showed agglomerations of nanospherical balls with Debye Scherrer's rings which correspond to the crystal lattice planes of TiO_2 while the elemental presence of the deposited nanoparticles were confirmed from the EDX studies.
- High transmittance percentage with optical band gap energy ranging from 3.41–3.60 eV was obtained.
- The chemical vibrational bonds existing between the nanoparticles and the band-to-band transitions and were evident from the FTIR and PL studies respectively.

ABSTRACT

Successive ionic layer adsorption and reaction (SILAR) method was adopted in synthesizing titanium dioxide nanoparticles at various temperatures so as to investigate their morphological, structural, elemental, optical, chemical bond and photoluminescence properties. The as-prepared nanoparticles were characterized with scanning electron microscopy (SEM), X-ray diffractometry (XRD), transmission electron microscopy (TEM), selected area electron diffractometer (SAED), energy dispersive x-ray spectroscopy (EDX), UV-Visible spectrophotometry (UV-Vis), photoluminescence (PL) spectra and fourier transform infrared spectroscopy (FTIR). Nanospherical balls revealing anatase and rutile crystal structures at (101) and (110) planes respectively were observed. Agglomerations of chain-like small particles manifested in Debye-Scherrer's rings were evident from the TEM and SAED patterns. EDX spectra confirmed the deposition of the major elements: Ti and O. High transmittance of about 80% with a band gap energy range of 3.41-3.60 eV was obtained from the optical properties. Emission peaks arising from the PL spectra gave information on the charge transport and recombination rates occurring at the TiO_2 nanoparticles while FTIR studies revealed the chemical vibrational bonds of the deposited TiO_2 NPs. The obtained results show the deposited nanoparticles are suitable for solar cell applications.

Keywords: SILAR, titanium dioxide, nanoparticles, transmittance, band gap.

1. INTRODUCTION

Titanium (IV) oxide or titanium dioxide or titania has the chemical formula TiO_2 and is the naturally occurring oxide of titanium. Titania is an efficient photocatalyst because it maintains its photostability over time, toxic-free and has high oxidizing power [1]. It occurs naturally as the minerals: anatase, rutile and brookite. The rutile crystallographic phase exhibits more stability and density than the anatase and brookite phases. The interface between rutile and anatase improves photocatalytic activity by increasing the separation of charge carriers [2]. When deposited as a thin film, TiO_2 serves as a good reflective optical coating due to its high refractive index. Other features like high transmission in the visible and near-infrared region, great usage in photocatalytic splitting of water, outstanding electrical (high resistivity and dielectric constant) and optical (optically transparent with high refractive index) features have increased its usage and research interest [1], [3]. Titanium dioxide has been synthesized via various methods like atomic layer epitaxy [4], electrophoretic method [5], dc magnetron sputtering [6]–[8], reactive r.f. magnetron sputtering [9], [10], ion beam enhanced deposition [11], calcination process [12], liquid phase deposition [1], [13], pulsed laser deposition [14]–[16], spray pyrolysis [17], [18], sol-gel [19]–[21], thermal evaporation [22], chemical vapor deposition [23], [24], chemical bath deposition (CBD) [25], [26], successive ionic layer adsorption and reaction (SILAR) [27]–[29]. SILAR method was adopted in this study because of its simplicity, no special equipment required, relatively cheap and ease in film thickness control, especially as it applies to optical devices. Titania finds application in protective layers of electronic devices, gas sensing material, photovoltaics, surface coatings to minimize wears, as an electric insulator and anti-reflective layer in optical coatings [19], [23].

However, few reports, though not recent have been made on TiO_2 nanoparticles synthesized by SILAR technique. Pathan *et al.*[28] synthesized titanium dioxide thin films via SILAR method using $TiCl_3$ and NH_4OH as cationic and anionic precursors, respectively. The films deposited on indium-doped tin oxide (ITO) substrates were annealed at 450 ^oC for 6 hours for annealing effect observation. Dense and uniform films were observed with the structure revealing only the beta-phase of the TiO_2 film. Elemental composition of deposit was confirmed while agglomerations were seen on the transmission electron microscopy images. Band gap energy of 3.0 eV with improved photo-activity upon annealing was obtained [27]. Patil *et al.* [29]

deposited TiO_2 thin films using 0.1 M $Ti(III)Cl_3$ as precursor, HCl as cation and NaOH as anion via SILAR method on fluorine-doped tin oxide and glass substrates in order to understand its structural, morphological, optical and photoactive properties. The films were annealed at 673 K for 2 hours in the air. A power conversion efficiency of 0.047% was obtained in 1 M NaOH electrolyte. Anatase phase was observed from the X-ray diffractomograms with the selected area electron diffraction (SAED) patterns confirming the diffraction planes of the nanocrystallites. Fourier transform infrared spectroscopy (FTIR) spectra revealed vibrational modes corresponding to the anatase phase with a band gap energy of 3.6 eV [28]. Park *et al.*[??] synthesized TiO_2 thin films and nanoparticles via SILAR method using $(NH_4)_2TiO(C_2O_4)_2.H_2O$ and NaOH as precursors. The films were put in a preheated box furnace at 200 ^oC (16 h), 400 ^oC (5 h), 600 ^oC (5 h), 800 ^oC (5 h) and 1000 ^oC (2 h) and characterized. The anatase and rutile phases were seen from the XRD patterns with homogenously closely packed TiO_2 thin films seen from the AFM images. The films annealed at 200 ^oC showed better mechanical stability and photocatalytic activity [29].

In this work, we present the morphological, structural, elemental and optical properties of titanium dioxide nanoparticles synthesized by SILAR method at annealing temperatures of 300 ^oC, 500 ^oC and 600 ^oC for 2 hours. SILAR method was adopted to regulate its thickness and encourage large scale production. No solvent was introduced unlike in previous reports so as to avoid contaminating the deposited layers and altering desired results. Alternatively, nanoparticles instead of thin films have been used so as to minimizing recombination effects, increasing surface area activity and increasing direct transition of the anatase phase.

2. EXPERIMENTAL DETAILS

TiO_2 nanoparticles were synthesized via SILAR method on glass substrates and annealing the obtained films at 300 ^oC, 500 ^oC and 600 ^oC respectively for 2 hours. The room-temperature SILAR method comprised of four (4) steps;

Step 1: In synthesizing the cationic solution, 4 ml of titanium isopropoxide ($Ti[OCH(CH_3)_2]_4$) was mixed in 25 ml of isopropanol ($CH_3CHOHCH_3$) in a beaker. 0.35 ml of hydrochloric (HCl) acid was mixed with 25 ml of isopropanol in another beaker. The solutions in both beakers were mixed together and stirred for about 10 minutes.

Step 2: 100 ml of distilled water in a beaker for rinsing film obtained from step 1

Step 3: In synthesizing the anionic solution, 0.01 M of sodium hydroxide (NaOH) solution was prepared and put in one beaker.

Step 4: 100 ml of distilled water in a beaker for rinsing film obtained from step 3

Cyclic Process: SILAR method was adopted in synthesizing the titanium dioxide films. The substrate was dipped in the cationic solution for 20 seconds for adsorption of the titanium species. Rinsing of substrate in distilled water for 5 seconds to remove loosely bound electrons. The substrate was then dipped in the anionic solution for 20 seconds and afterward rinsed in another beaker of distilled water for 5 seconds. The film formation continued until after 23 cycles where a feasible deposit was observed on the substrate surface. The titanium solution congealed after drying in a closed chamber for some hours. The synthesis process was repeated to obtain three different films which were annealed respectively at 300 ºC, 500 ºC and 600 ºC for 2 hours. Afterwards, the dried films were scraped off the substrate surfaces to obtain TiO_2 nanoparticles at different temperatures. The synthesis process is illustrated in Figure 1.

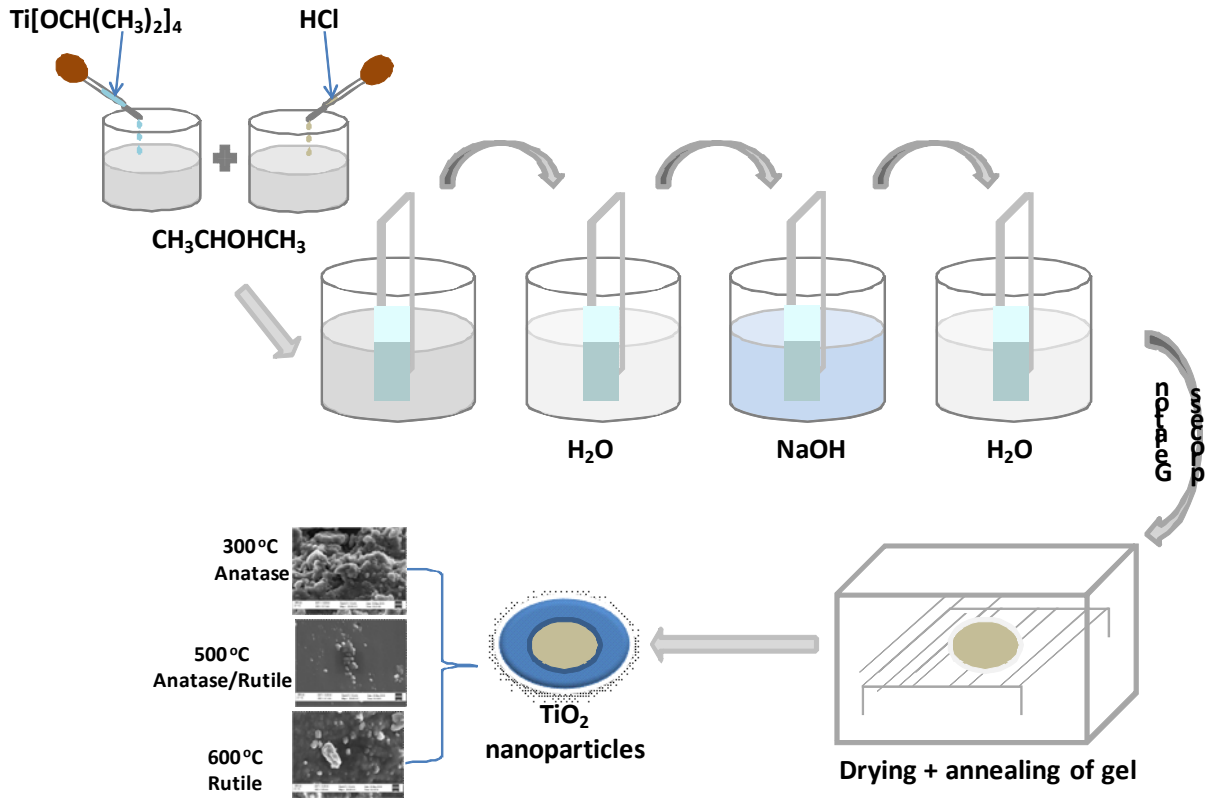

Figure 1: Illustration of the processes involved in synthesizing the TiO_2 nanoparticles.

During characterization of the nanoparticles, the morphological properties were obtained using a Zeiss scanning electron microscope while the structures were recorded using an x-ray diffractometer (Bruker AXS D8 diffractometer) at a scanning angle range from 10–90 º with Cu-K_α radiation of $\lambda = 1.5406$ Å. The average particle sizes were measured using Image J software. The elemental compositions were gotten using an energy dispersive x-ray (EDX) spectrometer while the optical properties were obtained using a QEP00503 spectrometer within a wavelength range of 300–2500 nm and 300-1200 nm respectively. Transmission electron microscopy (TEM) and selected area electron diffraction (SAED) studies were carried out using Tecnai G^2 F20 S-Twin High Resolution Transmission Electron Microscope (HRTEM) operated at 200 kV, the chemical vibrational bonds of the nanoparticles were studied from the fourier transform infrared (FTIR) spectrum using Thermo-Nicolet 8700 FTIR spectrometer while the photoluminescence (PL) properties were obtained from an F-7000 FL spectrophotometer model at a chopping speed of 40 Hz.

3.0 RESULTS AND DISCUSSION

3.1 Morphological Studies

Figure 2 shows the surface morphology of the TiO_2 nanoparticles synthesized at different annealing temperatures for 2 hours. The morphology reveals spherical balls of different sizes with dimensions in the nanometer range. Agglomerations have also been observed from the SEM images. The nanoparticles of different sizes spread uniformly across the surface for the purely anatase phase. This porous morphology was due to the nucleation and coalescence encountered during the formation process [28]. This morphology encourages photocatalytic activity as more species get adsorbed on the surface per unit area [7].

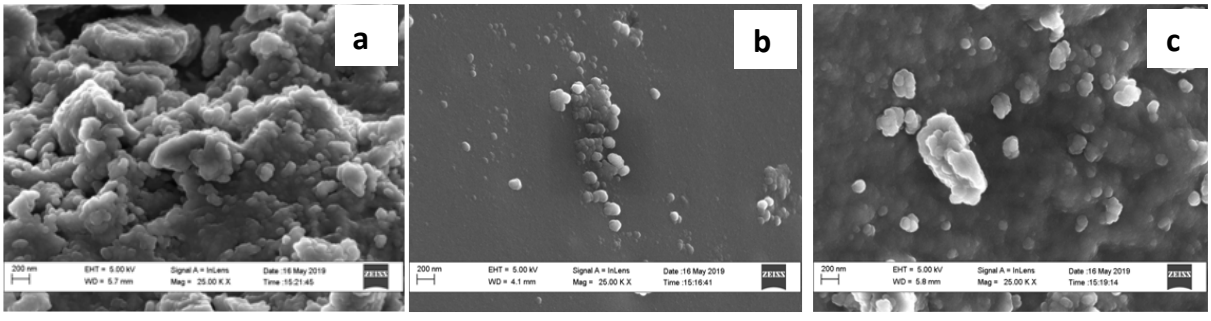

Figure 2: SEM micrographs of the TiO_2 films synthesized at (a) 300 ºC (b) 500 ºC and (c) 600 ºC

The average grain sizes of the TiO_2 films produced at 300 ºC, 500 ºC and 600 ºC were respectively 31.03 nm, 31.59 nm and 31.77 nm. It can be deduced that the average grain sizes of the films increased with annealing temperature. Increasing the annealing temperature also produced larger grain sizes with less surface coverage and smaller voids present. The different grain sizes are due to the nucleation and growth rates of the nanoparticles. The small voids obtained at higher temperatures increase the oxidation rate of the particles by allowing direct passage of oxygen molecules inward from the ambient surrounding [6]. Annealing titania enhances the adsorption of oxygen so that the anatase and rutile phases of the TiO_2 nanograins could be formed [22].

3.2 Structural Studies

Figure 3a shows the XRD patterns of the TiO_2 particles at various annealing temperatures with the corresponding indices of the different diffraction planes where A and R represent anatase and rutile respectively. The particles exhibited two phases: anatase and rutile. However, the particles annealed at 300 ºC showed the anatase phase, the particles annealed at 500 ºC exhibited both the anatase and the rutile phases while the particles annealed at 600 ºC showed a purely rutile phase. An increase in the diffraction intensity as the annealing temperature increased is an indication of crystallite growth and improved crystalline nature of the samples [1]. An increase in the magnitude of the diffraction peaks with increasing temperature could be because the radicals were adsorbed better into the materials synthesized at higher temperatures and with larger grain sizes [17]. At 300 ºC, the low intensities of the diffraction peaks were due to the transformation from amorphous to anatase phase that required sufficient temperature to initiate the crystallization process [1], [30]. Anatase-to-rutile phase transformations aimed at technological advancements have been studied by [31], [32]. The presence of the anatase phase makes it a potential material for photocatalytic applications while the rutile phase makes it applicable in medicine [5].

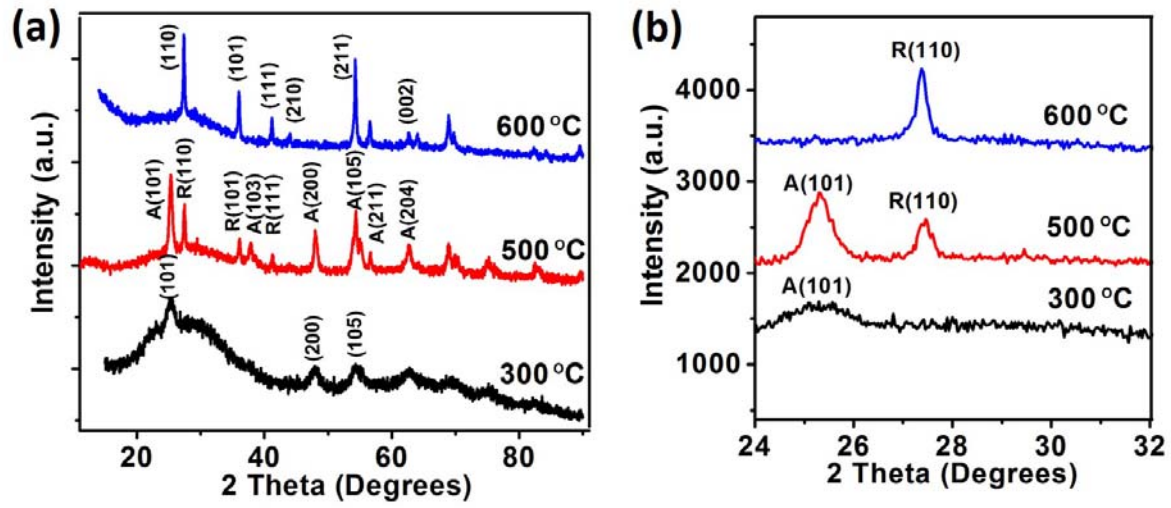

Figure 3: (a) XRD patterns of the TiO_2 particles at various annealing temperatures (b) Zoomed XRD patterns showing the most prominent anatase (A (101)) and rutile (R (110)) peaks.

The XRD patterns in Figure 3 reveal tetragonal crystal structures of the anatase and rutile TiO_2 phases corresponding to the JCPDS card numbers: 00-021-1272 and 00-021-1276 respectively. Upon increasing the temperature beyond 300 °C, (110) plane was prominently observed. The (110) plane of the stable rutile tetragonal phase at 600 °C exhibited the most intense peak. TiO_2 has been reported to be more stable with high manifestation of photocatalytic activity at (101) anatase planes [33].

From Figure 3b, as there are no apparent R (110) peaks for the particles annealed at 300 °C, hence its rutile structure content is assumed to be 0%. Similarly, for the particles annealed at 600 °C, the A (101) peaks are absent. Therefore, the rutile structure content is assumed to be 100%. However, for the 500 °C annealed sample, the anatase and rutile contents (f_A) and (f_R) in the materials were obtained to be 50.8% and 49.2% respectively using a formula proposed by Spurr and Myers [34] in equation (1).

$$f_A = \frac{1}{\left(1 + 1.26\left(I_R / I_A\right)\right)} \tag{1a}$$

$$f_R = 1 - f_A \tag{1b}$$

where I_A and I_R are the XRD intensities for A(101) and R(110) structures respectively.

This indicates that an increase in annealing temperature of TiO_2 brings about an amorphous-to-anatase-to-rutile transition. This agrees with research by Porter *et al.* [35] on the effect of calcination temperature on the structure on TiO_2.

The XRD results agree with the SEM results that increasing the annealing temperature led to an increase in the crystallinity of the material and hence an increase in the crystallite number. The average crystallite sizes of the nanoparticles for the prominent peaks were calculated using Scherrer's formula [36] in equation (2):

$$D = \frac{0.94\lambda}{\beta \cos\theta} \tag{2}$$

Where λ is the wavelength of the XRD target, θ is the Bragg's diffraction angle and β is the full width at half maximum (FWHM).

Crystal defects in the form of grain boundaries dislocations existed due to the polycrystalline nature of the titania nanoparticles. The lattice constants: a and c of the TiO_2 nanoparticles with other structural parameters are summarized in Table 1. The inter-planar distance, d, between parallel atomic planes and the dislocation density, δ, were obtained using equations (3) and (4) [37]:

$$d = \lambda / 2\sin\theta \tag{3}$$

$$\delta = \frac{1}{D^2} \tag{4}$$

Table 1: Summary of some crystal parameters obtained from the TiO_2 nanoparticles

Annealing Temperatures (°C)	**Crystallite Phase**	**FWHM (°)**	**D (nm)**	**d (nm)**	**δ (nm^{-2})**	**a**	**c**
300	A(101)	1.4266	0.1018	0.92	96.44	3.79	9.51
500	A(101)	0.5887	0.2468	0.92	16.42	3.79	9.51
500	R(110)	0.0978	0.3496	0.08	8.18	4.59	2.96
600	R(110)	0.2506	1.7975	0.08	0.31	4.59	2.96

It is evident from Table 1 that the 300 ^{o}C nanoparticles recorded the lowest crystallite size and agrees with the SEM results. The dislocation density of a material is inversely proportional to the crystallite size and is confirmed from the obtained results. The lattice constants correspond to the anatase and rutile phases of TiO_2 nanoparticles.

Transmission electron microscope (TEM) images and selected area electron diffraction (SAED) modes were obtained in imaging for the nanoparticles synthesized at various temperatures so as to respectively understand the morphological and crystallographic structures of the nanoparticles. Figure 4(a-b, d-e) describe the anatase phase while Figure 4(c, f) represent the rutile phase of the TiO_2 nanoparticles. The TEM patterns revealed agglomerations of small particles and chain-like crystallite aggregates viewed at the nanometer range. The different structures observed from the TEM images account for the different phases: anatase and rutile obtained from the XRD results. The interplanar spacing of the different samples revealing the anatase and rutile structures are indexed in the TEM patterns. The large surface area encompassing the porous nanospherical grains make the titania particles potential photoelectrochemical electrodes [28]. The SAED patterns in the figure revealed Debye-Scherrer rings with each ring representing a particular (h k l) reflection of either the anatase or rutile crystalline phases of the titania nanoparticles. The rings confirm the nanocrystalline nature of TiO_2 particles. The different arrangements of the diffracted rings show a phase evolution of the crystalline grains due to annealing. The anatase-to-rutile phase transformation was evident from the spots which became brighter with increasing temperature. The bright spots show preferential diffraction features while the high intensity of the spots show that it came from the nanoparticle core [7]. The spots also reveal the random orientation of the crystallites which correspond to different diffraction planes. The interplanar distances are indicated by rings which correspond to the lattice planes observed from the XRD patterns.

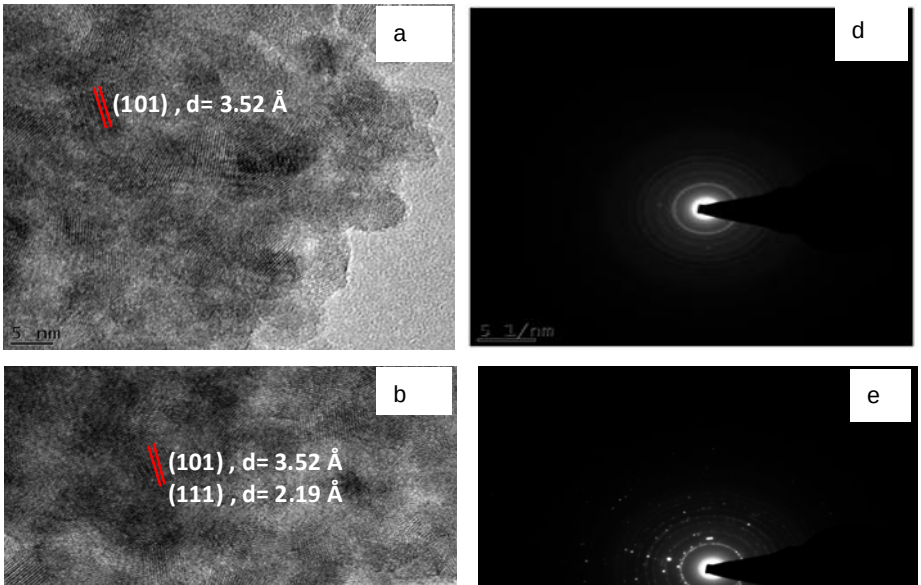

Figure 4: (a-c) TEM images and (d-f) SAED patterns of the TiO_2 nanoparticles synthesized respectively at a) 300 ºC b) 500 ºC c) 600 ºC

3.3 Elemental Composition

Energy dispersive x-ray spectroscopy (EDX or EDS) was adopted in determining the elemental composition of the synthesized TiO_2 particles. The EDX spectra of the TiO_2 nanoparticles annealed at various temperatures are shown in Figure 5. The major elements: titanium (Ti) and oxygen (O) were obtained and confirmed the deposition of the expected film. Other elements like: Cu, C and Si obtained could be due to environmental interferences during the laboratory synthesis process and the substrate used for the deposition. The EDX investigations confirmed the formation of TiO_2 nanoparticles upon deposition on the substrate surfaces.

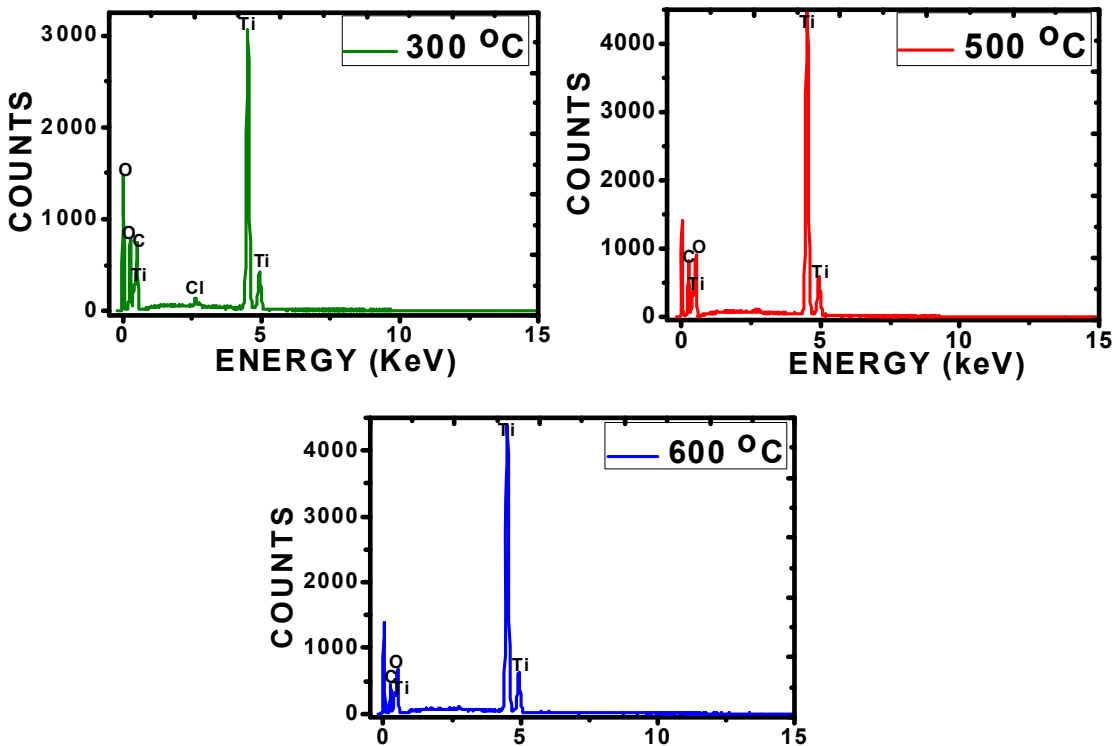

Figure 5: EDX spectra of TiO_2 nanoparticles synthesized at 300 ºC, 500 ºC and 600 ºC.

3.4 Optical Studies

Figure 6 shows the spectra of optical absorbance, transmittance and reflectance in the wavelength range 300-2500 nm of the TiO_2 particles annealed at different temperatures. The spectra showed interference fringes throughout the wavelength range. Low absorbance observed in the visible region of the electromagnetic spectra as seen in Figure 6(a) is the characteristic of TiO_2. Maximum transmittance of about 80% was obtained in Figure 6(b) at the highest annealing temperature. High transmittance percentage has also been obtained. The lower transmittance property of the particles annealed at temperatures of 300 ºC and 500 ºC could be due to sufficient oxygen vacancies that absorbed the incident light [11]. Excitation of the electrons from the valence to conduction band of titania after light absorption contributed to the low transmittance exhibited below 400 nm. The optical transmittance was also accompanied by a spectral blue shift in the lower wavelength regions. These transmittance properties could be attributed to annealing at high temperatures and transformations between anatase and rutile phases [38]. The rutile titania phase exhibited better optical transmittance. Figure 6(c) shows the particles deposited at lower temperatures recorded reduced reflectance than that synthesized at 600 ºC. Changes in the optical features could be due to slight changes in the crystallite size, phase structure and surface morphologies of the particles.

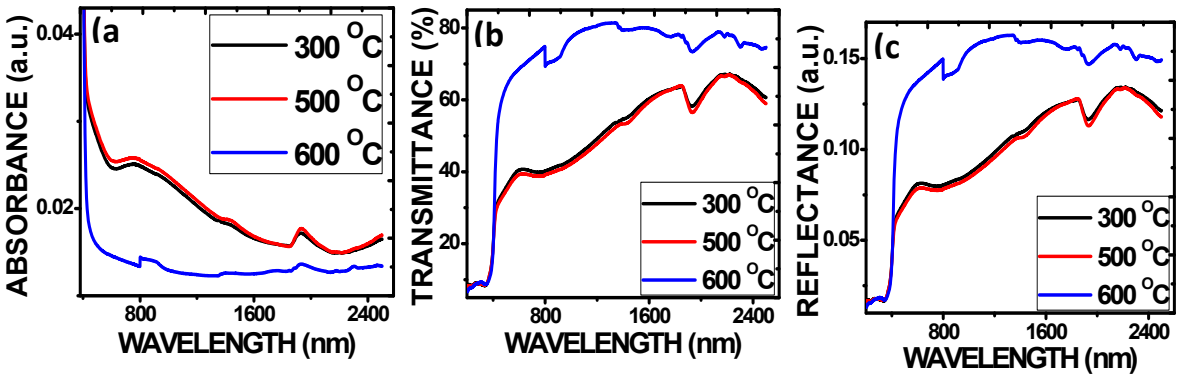

Figure 6: Plots showing the a) absorbance b) transmittance c) reflectance of the TiO_2 nanoparticles annealed at 300 ºC, 500 ºC and 600 ºC.

Figures 7(a) and (b) illustrate the absorption coefficient (α) and $(\alpha h\nu)^2$ (as a function of photon energy) synthesized at different temperatures. The plots were obtained from the diffuse reflectance values using Kubelka-Munk theory. The dependence of the absorption coefficient on the incident photon energy obtainable from Tauc equation helps in determining the nature of the optical absorption transition. The particles synthesized at 300 ºC and 500 ºC demonstrated lower absorption coefficients than that synthesized at 600 ºC. All the particles recorded higher absorption coefficients at the lower photon energy regions are shown in Figure 7(a). The increased absorption coefficient values at increasing temperatures agree with previous reports and could be due to increased crystallinity and compactness of the nanoparticles [6], [38]. The decrease in the absorption edge wavelength for the titania nanoparticles is a clear indication that its band gap would reduce with decreasing annealing temperature.

The Kubelka-Munk (K-M) equation is given in equation (5a) while the optical band gap energy (E_g) and absorption coefficient is related by equation (5):

$$F(R) = (1-R)^2 / 2R \qquad (5a)$$

$$(\alpha h\nu)^2 = A(h\nu - E_g)^n \qquad (5b)$$

Where F(R) is the K-M function, R is the diffuse reflectance, α is the absorption coefficient, hν is the photon energy, A is a factor that is dependent on the transition probability, h is Planck's

constant, and the power n depends on the transition during the absorption process. n has values ranging from 1/2, 3/2, 2, and 3 for the direct allowed, direct forbidden, indirect allowed, and indirect forbidden transition respectively. The nanoparticles synthesized at 300 ºC, 500 ºC and 600 ºC recorded band gap energies of 3.60 eV, 3.53 eV and 3.41 eV respectively as seen in Figure 6(b). Reduction of band gap energies with annealing temperature has been attributed to a reduction in interatomic spacing and structural modifications [6], [9]. Similar band gap energies have also been obtained [25], [28]. The higher band gap energies obtained could be due to quantum size effect [28] and the thermal stress encountered during the annealing process [14]. The reduction of the band gap energies at increasing temperatures justifies the increase in grain sizes as seen from the SEM images.

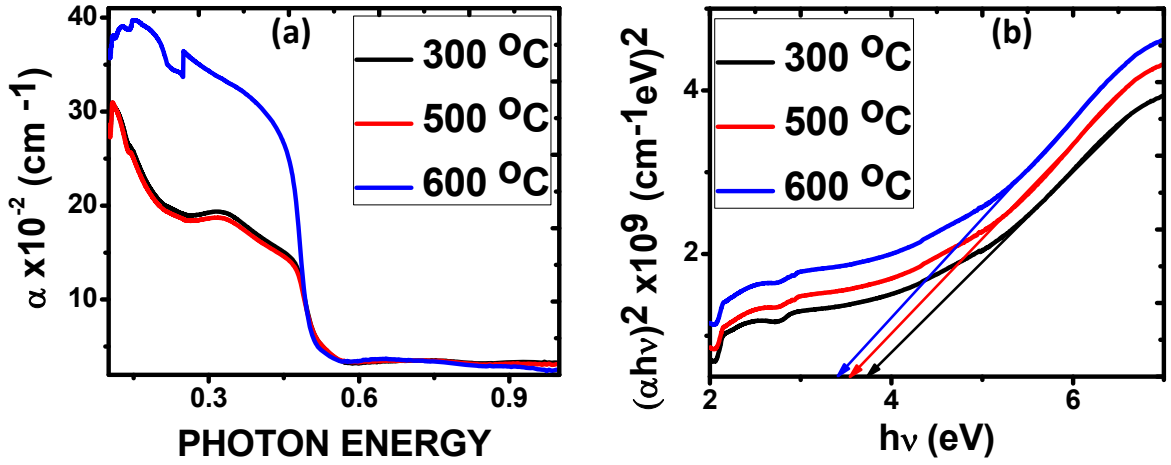

Figure 7: Optical plots showing the a) absorption coefficient and b) band gap energy of the nanoparticles synthesized at various temperatures.

3.5 Fourier transform infrared spectroscopy (FTIR)

FTIR study was carried out to investigate the chemical structure and vibrational bonds existing between the TiO_2 nanoparticles. The FTIR spectra of the TiO_2 nanoparticles synthesized at 300 ºC, 500 ºC and 600 ºC are shown in Figure 8. The samples show the main bands at 400-700 cm^{-1} which are attributed to Ti-O stretching and Ti-O-Ti bridging stretching modes [44]. The 1400-1750 cm^{-1} regions belong to O-H bending vibrations [45]. The broad bands at 2800-3800 cm^{-1}

represent the O-H vibration for water molecules while the broad band at 3100-3600 cm^{-1} is attributed to Ti-OH [1]. The O-H group was evident because of water molecule absorption from the aqueous solution during the synthesis process. The different phases: anatase and rutile were evident from the spectrum displayed by each sample. These results agree with the x-ray diffractomograms. The intensities of O-H vibration band reduced while that of the Ti-O band increased with annealing temperature. The results confirm the formation of titanium nanoparticles.

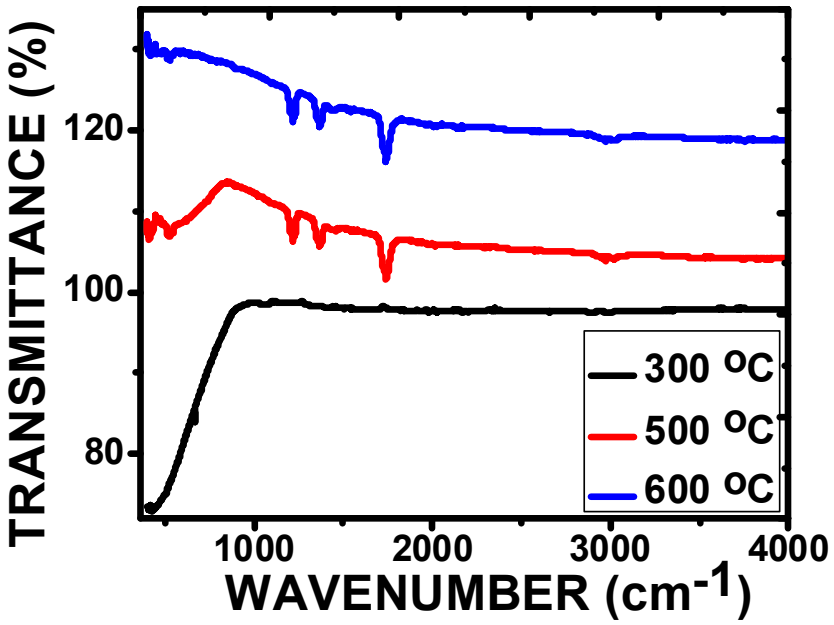

Figure 8: FTIR spectra of the TiO_2 nanoparticles synthesized at300 ºC, 500 ºC and 600 ºC.

3.6 Photoluminescence (PL) Studies

The PL emission spectrum is a useful tool in determining efficient charge transport and the rate of recombination of carriers in semiconductors [39]. Some reports on the PL spectra of titania nanoparticles have been presented in literature [25], [40], [41]. Figure 9(a) shows the room temperature photoluminescence spectra for the TiO_2 particles annealed at 300 ºC, 500 ºC and 600

ºC in the wavelength range of 350-1200 nm. Three main emission peaks were observed at 440 nm, 625 nm and 835 nm for the particle synthesized at 600 ºC while the particles synthesized at 300 ºC and 500 ºC had emission peaks at 430 nm and 695 nm. The broad bands in the visible region could arise due to the recombination of ionized oxygen vacancies with photo-generated holes. The observed peak at 430 nm corresponds to the band transitions due to electron excitation from the valence to the conduction band. All the particles manifested narrow and less intense emission peak at 620 nm. The emission peaks could be due to charge-transfer and band gap transitions [42]. The variations in the photoluminescence intensity could be due to a change in defect state of the titania surface and the different phase structures that arose from different annealing temperatures [43]. The particle synthesized at 600 ºC recorded the maximum emission intensity as compared to the other samples synthesized at lower temperatures. An illustration of the active energy levels of the materials is shown in Figure 9(b).

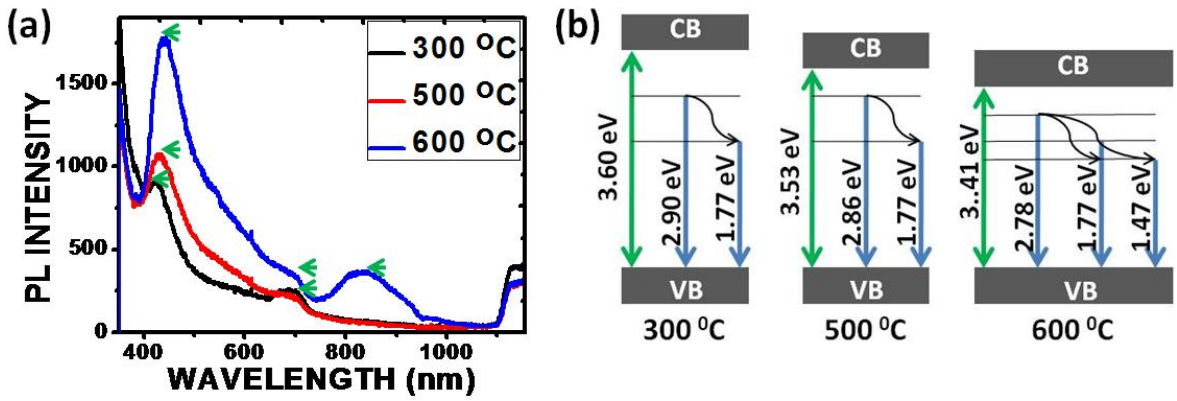

Figure 9: (a) Photoluminescence spectra showing the absorption emission peaks (green arrow) and (b) Illustration of active energy level for the TiO_2 nanoparticles synthesized at 300 ºC, 500 ºC and 600 ºC.

4.0 CONCLUSION

This study investigated the morphological, structural, elemental, optical and charge transport properties of TiO_2 nanoparticles synthesized by SILAR method at annealing temperatures of 300 ºC, 500 ºC and 600 ºC. SEM results revealed nanospherical porous grains with the anatase and rutile TiO_2 phases evident from the XRD results. EDX spectra confirmed the deposition of basic

elements on the substrate surface. Good optical properties with band gap energies ranging from 3.41 eV to 3.60 eV was obtained for the nanoparticles. TEM images showed agglomerations of small chain-like particles while SAED measurements confirmed the nanocrystalline nature of the deposited samples. PL measurements described the charge transport mechanisms while the FTIR studies revealed the chemical vibrational bonds existing between the TiO_2 nanoparticles. The rutile TiO_2 phase exhibited better features than the anatase phase of the nanoparticles. The deposited films have the potential in finding the applications in biomedicine and solar cells.

Acknowledgments

ACN (90406558) and FIE (90407830) graciously acknowledge UNISA for Postdoc and VRSP Fellowship awards respectively. We graciously acknowledge the grant by NCC under contract number NCC/R& D/UNN/014. Also, we thank Engr. Emeka Okwuosa for the generous sponsorship of April 2014, July 2016 and July 2018 Conference/ Workshops on Applications of Nanotechnology to Energy, Health & Environment conference.

Appendix A. Supplementary material

Supplementary data to this article can be found online at https://doi.org/10.1016/j.inoche.2019.107705.

REFERENCES

[1] J.-G. Yu, H.-G. Yu, B. Cheng, X.-J. Zhao, J. C. Yu, and W.-K. Ho, "The Effect of Calcination Temperature on the Surface Microstructure and Photocatalytic Activity of TiO2 Thin Films Prepared by Liquid Phase Deposition," *J. Phys. Chem. B*, vol. 107, no. 50, pp. 13871–13879, Dec. 2003.
[2] "Titanium dioxide," *Wikipedia*. 16-May-2019.
[3] S. Yamabi and H. Imai, "Crystal Phase Control for Titanium Dioxide Films by Direct Deposition in Aqueous Solutions," *Chem. Mater.*, vol. 14, no. 2, pp. 609–614, Feb. 2002.
[4] M. Ritala, M. Leskelä, E. Nykänen, P. Soininen, and L. Niinistö, "Growth of titanium dioxide thin films by atomic layer epitaxy," *Thin Solid Films*, vol. 225, no. 1, pp. 288–295, Mar. 1993.
[5] T. Moskalewicz, A. Czyrska-Filemonowicz, and A. R. Boccaccini, "Microstructure of nanocrystalline TiO2 films produced by electrophoretic deposition on Ti–6Al–7Nb alloy," *Surf. Coat. Technol.*, vol. 201, no. 16, pp. 7467–7471, May 2007.

[6] C.-C. Ting, S.-Y. Chen, and D.-M. Liu, “Structural evolution and optical properties of TiO2 thin films prepared by thermal oxidation of sputtered Ti films,” *J. Appl. Phys.*, vol. 88, no. 8, pp. 4628–4633, Sep. 2000.
[7] L. Dreesen, J.-F. Colomer, H. Limage, A. Giguère, and S. Lucas, “Synthesis of titanium dioxide nanoparticles by reactive DC magnetron sputtering,” *Thin Solid Films*, vol. 518, no. 1, pp. 112–115, Nov. 2009.
[8] K.-S. Lee and I.-S. Park, “Anatase-phase titanium oxide by low temperature oxidation of metallic Ti thin film,” *Scr. Mater.*, vol. 48, no. 6, pp. 659–663, Mar. 2003.
[9] N. Martin, C. Rousselot, D. Rondot, F. Palmino, and R. Mercier, “Microstructure modification of amorphous titanium oxide thin films during annealing treatment,” *Thin Solid Films*, vol. 300, no. 1, pp. 113–121, May 1997.
[10] M. D. Wiggins, M. C. Nelson, and C. R. Aita, “Phase development in sputter deposited titanium dioxide,” *J. Vac. Sci. Technol. A*, vol. 14, no. 3, pp. 772–776, May 1996.
[11] F. Zhang *et al.*, “Highly oriented rutile-type TiO2 films synthesized by ion beam enhanced deposition,” *J. Vac. Sci. Technol. A*, vol. 15, no. 4, pp. 1824–1827, Jul. 1997.
[12] P. de Almeida *et al.*, “Microstructure characterization of titanium dioxide nanodispersions and thin films for dye-sensitized solar cell devices,” *Appl. Phys. A*, vol. 79, no. 7, pp. 1819–1828, Nov. 2004.
[13] S. Deki, Y. Aoi, O. Hiroi, and A. Kajinami, “Titanium (IV) Oxide Thin Films Prepared from Aqueous Solution,” *Chem. Lett.*, vol. 25, no. 6, pp. 433–434, Jun. 1996.
[14] Y. Du *et al.*, “Optical properties of SrTiO3 thin films by pulsed laser deposition,” *Appl. Phys. A*, vol. 76, no. 7, pp. 1105–1108, May 2003.
[15] E. György, G. Socol, E. Axente, I. N. Mihailescu, C. Ducu, and S. Ciuca, “Anatase phase TiO2 thin films obtained by pulsed laser deposition for gas sensing applications,” *Appl. Surf. Sci.*, vol. 247, no. 1, pp. 429–433, Jul. 2005.
[16] N. Koshizaki, A. Narazaki, and T. Sasaki, “Preparation of nanocrystalline titania films by pulsed laser deposition at room temperature,” *Appl. Surf. Sci.*, vol. 197–198, pp. 624–627, Sep. 2002.
[17] L. Castañeda, J. C. Alonso, A. Ortiz, E. Andrade, J. M. Saniger, and J. G. Bañuelos, “Spray pyrolysis deposition and characterization of titanium oxide thin films,” *Mater. Chem. Phys.*, vol. 77, no. 3, pp. 938–944, Jan. 2003.
[18] D. R. Acosta, A. I. Martínez, A. A. López, and C. R. Magaña, “Titanium dioxide thin films: the effect of the preparation method in their photocatalytic properties,” *J. Mol. Catal. Chem.*, vol. 228, no. 1, pp. 183–188, Mar. 2005.
[19] T. Houzouji, N. Saito, A. Kudo, and T. Sakata, “Electroluminescence of TiO2 film and TiO2:Cu2+ film prepared by the sol-gel method,” *Chem. Phys. Lett.*, vol. 254, no. 1, pp. 109–113, May 1996.
[20] R. S. Sonawane, S. G. Hegde, and M. K. Dongare, “Preparation of titanium(IV) oxide thin film photocatalyst by sol–gel dip coating,” *Mater. Chem. Phys.*, vol. 77, no. 3, pp. 744–750, Jan. 2003.
[21] C. Garzella, E. Comini, E. Tempesti, C. Frigeri, and G. Sberveglieri, “TiO2 thin films by a novel sol–gel processing for gas sensor applications,” *Sens. Actuators B Chem.*, vol. 68, no. 1, pp. 189–196, Aug. 2000.
[22] D. Manno, G. Micocci, R. Rella, A. Serra, A. Taurino, and A. Tepore, “Titanium oxide thin films for NH3 monitoring: Structural and physical characterizations,” *J. Appl. Phys.*, vol. 82, no. 1, pp. 54–59, Jul. 1997.

[23] H. Ha, M. Yoshimoto, H. Koinuma, B. Moon, and H. Ishiwara, “Open air plasma chemical vapor deposition of highly dielectric amorphous TiO2 films,” *Appl. Phys. Lett.*, vol. 68, no. 21, pp. 2965–2967, May 1996.
[24] I. Djerdj, A. M. Tonejc, M. Bijelić, V. Vranes˘a, and A. Turković, “Transmission electron microscopy studies of nanostructured TiO2 films on various substrates,” *Vacuum*, vol. 80, no. 4, pp. 371–378, Oct. 2005.
[25] G. Govindasamy, P. Murugasen, S. Sagadevan, G. Govindasamy, P. Murugasen, and S. Sagadevan, “Investigations on the Synthesis, Optical and Electrical Properties of TiO2 Thin Films by Chemical Bath Deposition (CBD) method,” *Mater. Res.*, vol. 19, no. 2, pp. 413–419, Apr. 2016.
[26] A. H. Mayabadi *et al.*, “Evolution of structural and optical properties of rutile TiO2 thin films synthesized at room temperature by chemical bath deposition method,” *J. Phys. Chem. Solids*, vol. 75, no. 2, pp. 182–187, Feb. 2014.
[27] H. M. Pathan, S.-K. Min, J. D. Desai, K.-D. Jung, and O.-S. Joo, “Preparation and characterization of titanium dioxide thin films by SILAR method,” *Mater. Chem. Phys.*, vol. 97, no. 1, pp. 5–9, May 2006.
[28] U. M. Patil, K. V. Gurav, O.-S. Joo, and C. D. Lokhande, “Synthesis of photosensitive nanograined TiO2 thin films by SILAR method,” *J. Alloys Compd.*, vol. 478, no. 1, pp. 711–715, Jun. 2009.
[29] S. Park, E. DiMasi, Y.-I. Kim, W. Han, P. M. Woodward, and T. Vogt, “The preparation and characterization of photocatalytically active TiO2 thin films and nanoparticles using Successive-Ionic-Layer-Adsorption-and-Reaction,” *Thin Solid Films*, vol. 515, no. 4, pp. 1250–1254, Dec. 2006.
[30] S. Rajesh Kumar, C. Suresh, A. K. Vasudevan, N. R. Suja, P. Mukundan, and K. G. K. Warrier, “Phase transformation in sol–gel titania containing silica,” *Mater. Lett.*, vol. 38, no. 3, pp. 161–166, Feb. 1999.
[31] G. B. Song, J. K. Liang, F. S. Liu, T. J. Peng, and G. H. Rao, “Preparation and phase transformation of anatase–rutile crystals in metal doped TiO2/muscovite nanocomposites,” *Thin Solid Films*, vol. 491, no. 1, pp. 110–116, Nov. 2005.
[32] A. Weibel, R. Bouchet, P. Bouvier, and P. Knauth, “Hot compaction of nanocrystalline TiO2 (anatase) ceramics. Mechanisms of densification: Grain size and doping effects,” *Acta Mater.*, vol. 54, no. 13, pp. 3575–3583, Aug. 2006.
[33] L. Chu, Z. Qin, J. Yang, and X. Li, “Anatase TiO_2 Nanoparticles with Exposed {001} Facets for Efficient Dye-Sensitized Solar Cells,” *Sci. Rep.*, vol. 5, p. 12143, Jul. 2015.
[34] R. A. Spurr and H. Myers, “Quantitative analysis of anatase-rutile mixtures with an X-ray diffractometer,” *Anal. Chem.*, vol. 29, no. 5, pp. 760–762, 1957.
[35] J. F. Porter, Y.-G. Li, and C. K. Chan, “The effect of calcination on the microstructural characteristics and photoreactivity of Degussa P-25 TiO2,” *J. Mater. Sci.*, vol. 34, no. 7, pp. 1523–1531, 1999.
[36] A. C. Nkele *et al.*, “Role of metallic dopants on the properties of copper (1) iodide nanopod-like structures,” *Vacuum*, vol. 161, pp. 306–313, Mar. 2019.
[37] O. O. Apeh *et al.*, “Properties of nanostructured ZnO thin films synthesized using a modified aqueous chemical growth method,” *Mater. Res. Express*, 2018.
[38] M. H. Suhail, I. M. Ibrahim, and G. M. Rao, “Characterization and gas sensitivity of cadmium oxide thin films prepared by thermal evaporation technique,” *J. Electron Devices*, vol. 13, pp. 965–974, 2012.

[39] X. Z. Li, F. B. Li, C. L. Yang, and W. K. Ge, “Photocatalytic activity of WOx-TiO2 under visible light irradiation - ScienceDirect,” 2001. [Online]. Available: https://www.sciencedirect.com/science/article/abs/pii/S1010603001004464. [Accessed: 24-Jun-2019].
[40] B. Zhou, L. Xiao, and T. J. Li, “Absorption redshift in TiO2 ultrafine particles with surfacial dipole layer,” 1991. [Online]. Available: https://aip.scitation.org/doi/abs/10.1063/1.106211. [Accessed: 24-Jun-2019].
[41] N. Bai, S. Li, H. Chen, and W. Pang, “Preparation, characterization and photoluminescence properties of mesolamellar titanium dioxide films,” 2001. [Online]. Available: https://pubs.rsc.org/en/content/articlelanding/2001/jm/b103930j/unauth#!divAbstract. [Accessed: 24-Jun-2019].
[42] F. B. Li and X. Z. Li, “The enhancement of photodegradation efficiency using Pt–TiO2 catalyst,” *Chemosphere*, vol. 48, no. 10, pp. 1103–1111, Sep. 2002.
[43] F. B. Li and X. Z. Li, “Photocatalytic properties of gold/gold ion-modified titanium dioxide for wastewater treatment,” *Appl. Catal. Gen.*, vol. 228, no. 1, pp. 15–27, Mar. 2002.
[44] A. M. Peiró, J. Peral, C. Domingo, X. Domènech, and J. A. Ayllón, “Low-Temperature Deposition of TiO2 Thin Films with Photocatalytic Activity from Colloidal Anatase Aqueous Solutions,” *Chem. Mater.*, vol. 13, no. 8, pp. 2567–2573, Aug. 2001.
[45] H. Y. Y. Ko, M. Mizuhata, A. Kajinami, and S. Deki, “Fabrication of high performance thin films from metal fluorocomplex aqueous solution by the liquid phase deposition,” *J. Fluor. Chem.*, vol. 120, no. 2, pp. 157–163, Apr. 2003.